

Development of Micro-Electrode Array Sensors for Electrochemical Detection of Dissolved Oxygen

by

Hanna Marie Hansen

An undergraduate thesis advised by

Dr. Ethan D. Minot

submitted to

Department of Physics, Oregon State University

in partial fulfilment of the requirements for the degree of

Baccalaureate of Science in Physics

Submitted on May 8th, 2020

Abstract

Microelectrode array (MEA) dissolved-oxygen (DO) sensors were built and electrochemically tested in a solution of potassium ferricyanide. MEAs are becoming more popular as DO sensors because of their small size and capacity for simultaneous measurements with multiple recording sites. The ability to measure DO with multiple recording sites is useful for monitoring systems such as biofilm metabolism, which is an important factor in wastewater treatment. MEAs are beneficial because they are less destructive than individual microelectrodes that need to be moved through a sample to collect multiple measurements.

The MEA used in the present work used gold electrodes, and a separate silver/silver chloride wire was used as the counter/reference electrode. The ferri/ferrocyanide redox couple is a reversible reaction with a well-known electrochemical behavior, making it a good way to test the electrochemical functionality of the MEA before using it to measure DO. Voltage was applied to the gold electrode in potassium ferricyanide solution, which initiated a redox reaction. The movement of electrons increases with the number of redox reactions occurring, meaning that measured current increases proportionally to the concentration of ions that get oxidized or reduced. The experiments were done inside a Faraday cage to minimize noise, and cyclic voltammograms were collected.

There was a good linear response to the potassium ferricyanide, and the data was close to what was predicted by the Randles-Sevcik equation. The shape of the cyclic voltammograms appeared to have the characteristics of a reversible reaction, but the difference in voltage between the two peak currents was higher than expected. This may be due to an extra voltage drop at the counter electrode that is independent of the reactions, or high resistance due to inadequate electrolyte concentrations. Other possible interfering factors include adsorption at the electrodes and solution composition. The linear response of the sensor and its agreement with the Randles-Sevcik equation are promising signs that the sensor can measure differences in concentration, but a better understanding of what factors interfere with measurements is needed before applying the MEA to measuring DO concentrations.

Table of Contents

List of Figures	1
Chapter 1 –Introduction	2
1.1 Overview.....	2
1.2 Background.....	3
1.2.1 Polarographic dissolved-oxygen sensor.....	3
1.2.2 Electrochemical reactions	5
1.2.3 Cyclic voltammetry.....	6
1.2.4 Photolithography.....	9
Chapter 2 –Methods.....	11
2.1 Fabrication of wax-coated wire electrodes.....	11
2.2 Fabrication of micro-electrode array.....	12
2.3 Electrochemical analysis	13
Chapter 3 –Results & Discussion.....	16
3.1 Dissolved oxygen cyclic voltammograms.....	17
3.2 Potassium ferricyanide cyclic voltammograms.....	20
Chapter 4 –Conclusion.....	26
Acknowledgements.....	27
References.....	28

List of Figures

Chapter 1 - Introduction

1.1 Neural micro-electrode array (MEA).....	2
1.2 Cross-section of a two-electrode polarographic DO sensor.....	4
1.3 Cathodic current versus applied voltage with respect to a calomel electrode.....	6
1.4 DO sensor calibration technique.....	8
1.5 Photolithography technique and MEA DO sensor example.....	9

Chapter 2 - Methods

2.1 Wax-coated gold electrode.....	12
2.2 Photolithography technique.....	12
2.3 Electronic setup of DO sensors.....	15

Chapter 3 – Results & Discussion

3.1 Background noise inside and outside of a faraday cage.....	16
3.2 Cyclic voltammograms of wire electrode DO sensor.....	18
3.3 Cyclic voltammograms of wire electrode in potassium ferricyanide.....	20
3.4 Cyclic voltammograms of MEA in potassium ferricyanide.....	21
3.5 Experimental peak currents and Randles – Sevcik equation.....	23

Chapter 1 - Introduction

1.1. Overview

Electrochemical monitoring with microelectrodes is one of the most reliable tools to observe chemical dynamics of biological processes in living systems [1]. Microelectrodes have dimensions on the scale of microns and are more advantageous than conventional electrochemical electrodes due to their higher spatial resolution, faster response, and smaller double layer capacitance [1]. In recent years, interests have begun to shift toward arrays of microelectrodes because they keep the advantages of single microelectrodes, while including other advantages such as the capacity to take multiple simultaneous in-situ measurements. Being able to record simultaneous measurements with arrays is beneficial because it is less destructive than moving a single electrode through a living sample.

A current application of micro-electrode arrays (MEAs) is neuron-recording devices and neural prosthesis to treat patients who have suffered sensory and motion injuries [2]. An example of a neural MEA (Utah array) can be seen in Figure 1.1, where each needle has multiple recording sites for simultaneous measuring of extracellular potentials from multiple neurons. Unlike the single electrode recording, multi-electrode arrays can monitor many neurons to observe interactions among distant neurons [3]. MEAs are also rising in popularity among other disciplines including biological and environmental research. A potential application of MEAs is to monitor the metabolic activity of biofilms.

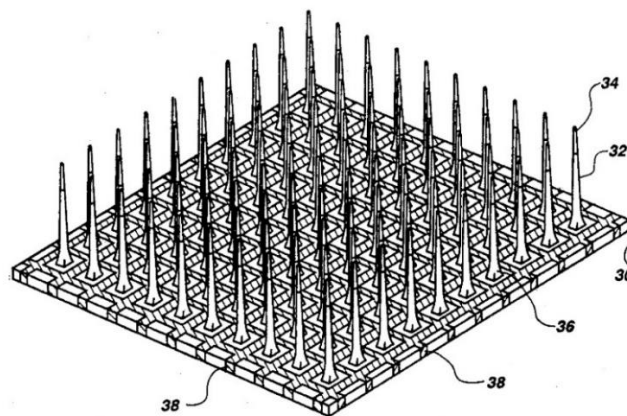


Figure 1.1 Micro Electrode Array (MEA) used to monitor neural signals. Adapted from Richard A. Normann's US Patent #5,215,088.

Biofilms are collections of microorganisms that can attach to a variety of surfaces. A characteristic of biofilms is that the microorganisms are suspended in a hydrated polymerized matrix which they self-generate [4]. Biofilms are proven to be quite useful as bioremediators in wastewater treatment. Being able to monitor biofilm activity will give a better understanding of how varying microbial environments will affect their metabolic efficiency, which is important for the development of new bioremediation strategies.

A well-established method of recording the concentration of dissolved oxygen in a liquid sample is with a polarographic dissolved oxygen (DO) sensor. Polarographic DO sensors use oxygen reduction reactions, which are reactions involving the transfer of electrons, to determine oxygen concentration by measuring current. Dissolved oxygen molecules undergo a reduction reaction at a metal electrode, often gold or platinum, in the presence of an applied voltage. Since the transfer of electrons make an electrical current, one can correlate the magnitude of current to a corresponding oxygen concentration.

To integrate a DO sensor with biofilms, the polarographic oxygen sensor will have to be miniaturized onto an MEA chip. The present work outlines the methods for fabricating an MEA dissolved-oxygen sensor with future applications including direct integration with biofilms. To have a baseline to compare MEA measurements with, a simple setup using gold and silver wires as electrodes was used to collect preliminary data, and the MEA was tested in ferri/ferrocyanide solution. The ferri/ferrocyanide redox couple is a standard for testing electrochemical equipment because it has a well-known electrochemical behavior.

1.2. Background

1.2.1. Polarographic Dissolved-Oxygen Sensors

The MEA DO sensor functions much like a conventional electrochemical DO sensor. DO sensors indirectly measure dissolved oxygen concentration through correlating it to the current produced from a redox reaction. Redox reactions, or reduction-oxidation reactions, involve the transfer of electrons which by extension involves electric current. As illustrated in Figure 1.2, a polarographic oxygen sensor consists of two electrodes: a working electrode and a counter electrode. The working electrode is inert, meaning it does not participate in chemical reactions. A common inert material for this electrode is gold or platinum. The counter electrode material is

often silver/silver chloride, where the silver and chloride ions combine to produce the electrons used in the reduction of oxygen. Electrons travel from the silver electrode to the gold electrode where oxygen accepts the electrons for its reduction reaction. The direction of current described requires that the gold electrode is negatively polarized in relation to the silver electrode [5]. The concentration and diffusion rate of oxygen directly effects the magnitude of measured current.

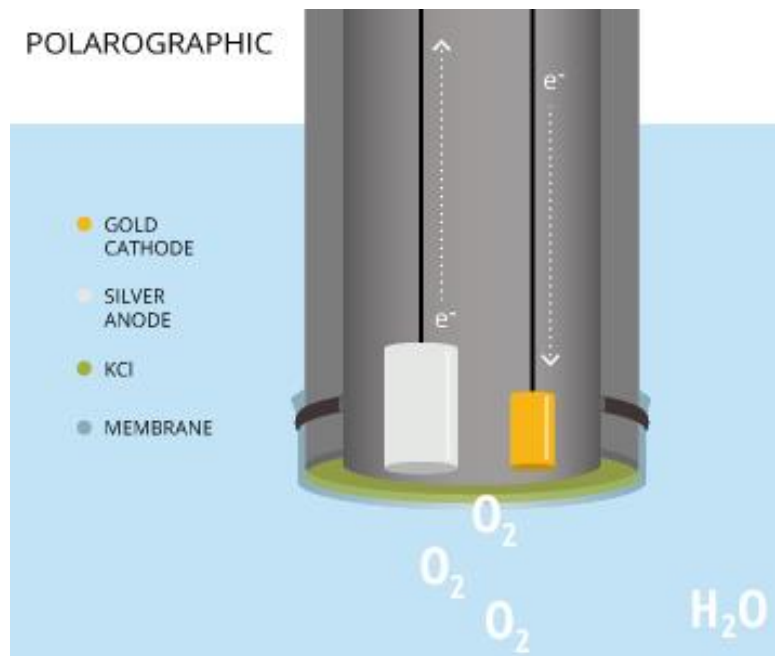


Figure 1.2 A cross section of a two-electrode polarographic commercial DO sensor. Oxygen accepts electrons and gets reduced at the gold electrode, and the electrolyte (KCl) contributes electrons to the silver electrode. This electrode is equipped with an oxygen permeable membrane to keep out other electrochemically active species. Adapted from [5].

Conventional DO sensors typically use an oxygen permeable membrane to regulate oxygen diffusion and block other electrochemically active species that may be present in the solution. For the purposes of the work in this paper, deionized water will be used as the solvent to reduce contaminants instead of an oxygen permeable membrane.

1.2.2. Electrochemical Reactions

Oxygen gets reduced at the gold cathode of a polarographic DO sensor. Reduction reactions involve the gain of electrons, and with every gain in electrons, there must be a loss of electrons. This loss of electrons comes from the oxidation of the silver counter electrode. The half reaction at the silver electrode is

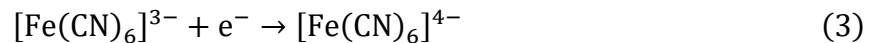


and the half reaction for the oxygen reduction at the gold electrode is

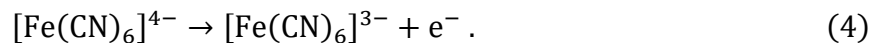


The electrolyte, KCl, allows for conductivity between the two electrodes [6], and contributes its chloride ion to the oxidation reaction at the silver electrode, as described by Equation 1. This reaction becomes visible as a dark coating of silver chloride on the electrode after several DO measurements. The formation of the AgCl layer should be monitored because thick layers of silver chloride will degrade the electrode performance over time [5]. When the silver oxidizes, it produces electrons which pass through an external circuit and exit at the gold electrode, allowing for the reduction of oxygen to produce hydroxide ions as described by Equation 2.

Ferri/ferrocyanide ions ($[\text{Fe}(\text{CN})_6]^{3-} / [\text{Fe}(\text{CN})_6]^{4-}$) are a well-known reversible redox couple described by the following half reactions:



and



Equation 3 shows the reduction of ferricyanide to ferrocyanide, and equation 4 shows the oxidation of ferrocyanide to ferricyanide. Like DO, ferricyanide gets reduced at the gold electrode, while the ferrocyanide gets oxidized. This reaction is reversible because the electrons transfer quickly and unhindered [7].

1.2.3. Cyclic Voltammetry

Cyclic voltammetry is an electrochemical technique used to monitor reduction and oxidation reactions which consists of measuring the current that results from cycling the potential of the working electrode (against the counter electrode). The potential is swept negatively until it reaches the chosen maximum potential (cathodic trace), then the potential is applied in the positive direction until it returns to the initial potential (anodic trace). Electrochemical activity is monitored through analyzing the shape of the cyclic voltammogram, and the shapes vary based on the electrochemical species being measured. As shown in Figure 1.3, the cathodic trace of cyclic voltammograms related to DO are expected to show steep increase in current (oxygen reduction), followed by a plateau, and then another steep increase in current (other electrode reactions) [8].

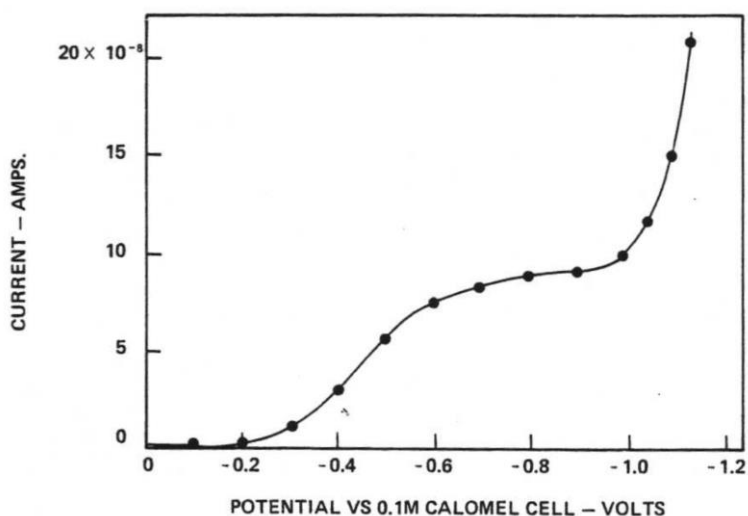


Figure 1.3 A measurement of cathodic current from an oxygenated solution with an applied voltage ranging from 0 V to -1.1 V (with respect to a calomel reference electrode). The solution was unbuffered, had a NaCl concentration of 0.1 M, and was kept at a temperature between 21.3 °C and 22 °C. Adapted from [8].

The initial increase in current is due to the oxygen being reduced at the electrode as a function of amount of voltage applied. Voltage and current are analogous to the flow of water due to a pressure gradient, where voltage can be thought of as an electron pressure gradient. The higher the potential, the greater the flow of electrons. In the presence of high oxygen concentration near the gold electrode surface, electrons will continue to flow at a rate proportional to the applied

voltage. As voltage is increased and the oxygen consumption rate increases, a depletion layer is formed around the surface of the gold electrode. The current then becomes a function of the diffusion rate of oxygen across this depletion layer. This can be modeled as

$$\mathbf{j} = -D_o \nabla c, \quad (3)$$

which can be written in the simplified form as

$$j = -D_o \frac{dc}{dx}, \quad (4)$$

where j is the flux of oxygen, D_o is the diffusion coefficient of oxygen in water, and $\frac{dc}{dx}$ is the concentration gradient in one dimension (perpendicular to the electrode surface) [8]. Notice that the flux of oxygen is the negative gradient because mass flow travels from high to low concentrations.

The formation of the depletion layer is represented in Figure 1.3 as the plateau region between approximately -0.6 V to -1.0 V. DO reduction in this region is limited by mass flow rate because the oxygen diffusion across the depletion layer is at its maximum described by Equation 3. In other words, oxygen is being consumed faster than it can be supplied through mass transfer.

When current is limited by the diffusion rate, the electrode is said to be *polarized*, meaning applied voltage can change with little effect on the measured current [8]. Polarographic DO sensors take measurements in the polarized region, hence their name. This allows for easy calibration of linear sweep graphs (a single voltage sweep in one direction) as described in Figure 1.4.

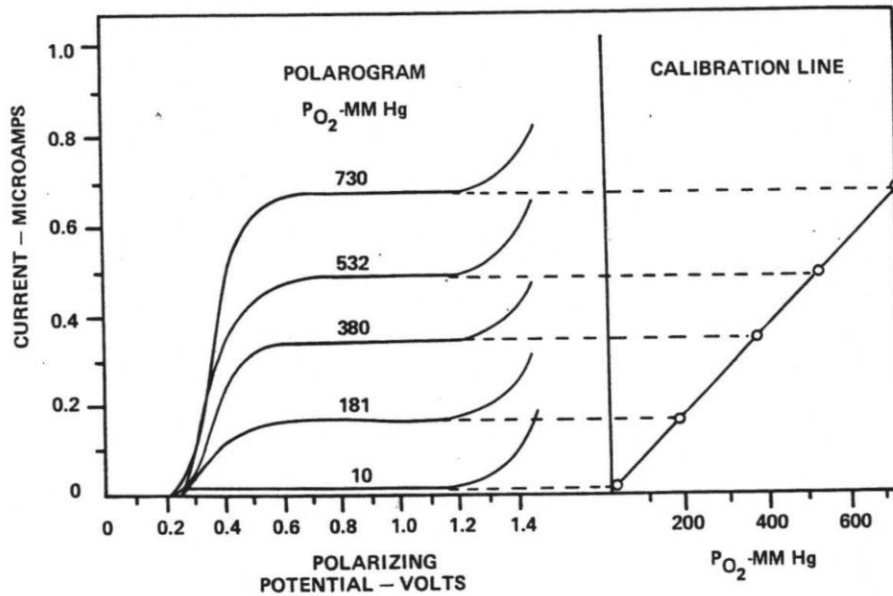


Figure 1.4 A technique for calibrating a polarographic DO sensor. The technique takes advantage of the plateau, or polarized region, where the current is stable and only limited by the diffusion rate of oxygen (ideally). In reality, the plateau would not be perfectly horizontal as depicted. Higher oxygen concentrations yield higher currents, as seen by the rising plateau. Each plateau current is plotted against its respective oxygen concentration to construct a calibration line. Adapted from [8].

The cathodic traces in Figure 1.4 are idealized for illustration purposes; the plateau region would never be perfectly horizontal due to small changes in current caused by minor variations in voltage. Many commercial DO sensors are equipped with a third electrode (reference electrode) that holds a voltage that is independent of both solution and current flow. The working gold electrode may then take measurements at a constant voltage in relation to the reference electrode, while the counter electrode ensures that no current passes through the reference electrode [9]. At moderately high DO concentrations, the small changes in current in the polarized region are small compared to the current produced by the DO reduction, and for the purposes of the experiment in this paper, a two-electrode system will suffice. With a material such as silver which has a well-known half-cell reaction with chloride, the counter electrode will simultaneously take on the role of a reference electrode.

1.2.4. Photolithography

Using the concepts discussed in previous sections, the electrode system can be miniturized into a micro-electrode array (MEA). The fabrication of an MEA with gold electrode patches and will involve transferring a geometric pattern from a photomask to a chip covered in a photo-reactive material, which is a technique known as photolithography. An example schematic of the photolithography process used in the fabrication of an MEA DO sensor needle can be seen in Figure 1.5.

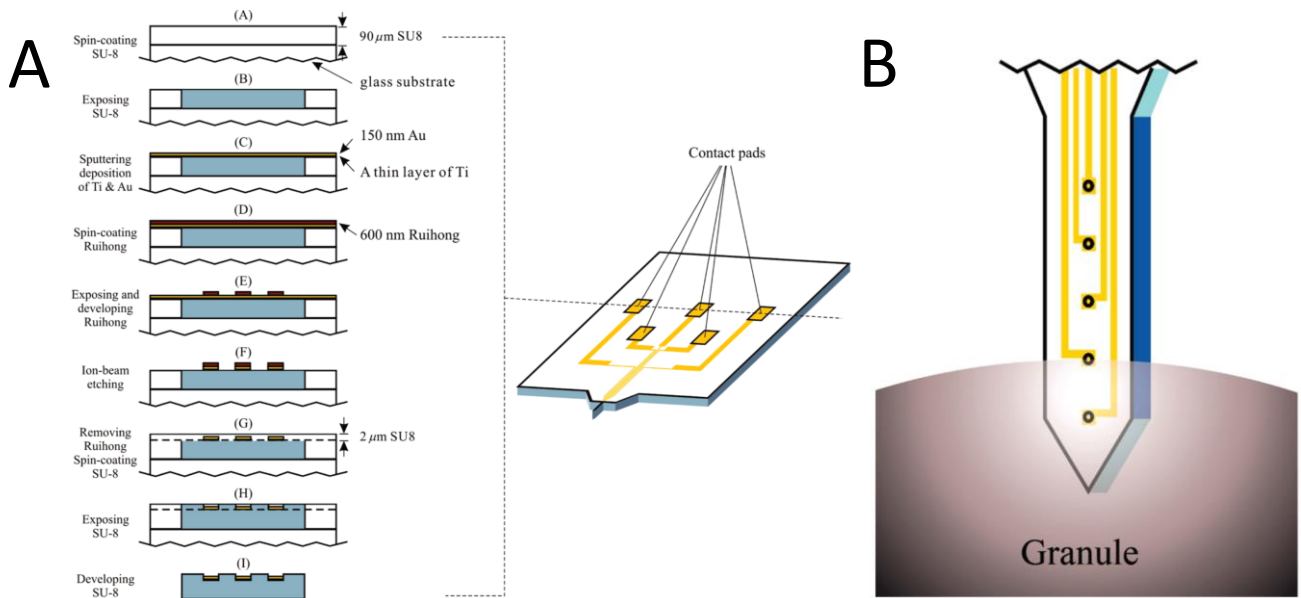


Figure 1.5 A) Schematic diagram of a photolithography technique for the fabrication of a needle MEA used to monitor DO concentrations in an aerobic granule (a granule containing microbes). B) An illustration of the MEA needle position in an aerobic granule. The needle has five electrodes to simultaneously measure DO concentrations with multiple distances from the granule surface. Adapted from [10].

A notable paper by Liu et al. described a procedure for making novel MEA DO sensors to monitor bacteria contained in aerobic granules [10]. Photolithography was used to fabricate the sensors as described in Figure 1.2 A, and the granules were monitored with a needle shaped MEA as illustrated in Figure 1.2 B. In this case, Liu et. al. patterned a glass substrate using SU-8 as the photoresist on which a thin layer of gold was distributed. A new layer of photoresist, this time Ruihong, was placed on top of the gold, and UV exposure through a photomask left behind the desired pattern of photoresist. Ion-beam etching was then used to remove the uncovered gold.

A new layer of SU-8 was placed, and the excess photoresist covering the leftover gold got removed, leaving a chip with exposed gold patches. After fabricating the MEA DO sensor chip, the paper by Liu et al. showed that they were able to measure the oxygen concentration in an aerobic granule. Figure 1.2 B shows the placement of the MEA needle used in the paper by Liu et al. The MEA consists of five electrodes for simultaneous measurements of the dissolved oxygen in the surrounding environment of the aerobic granule.

A procedure similar to photolithography technique outlined above will be used to fabricate the sensor in the present work. Instead of a needle, the proposed chip design will be a flat surface with exposed gold to function as the electrode and the location where oxygen reacts.

Chapter 2 –Methods

2.1. Fabrication of Wax-Coated Wire Electrodes

The preparation of electrodes used in the preliminary experiment involved a gold wire, silver wire, and candle wax.

The silver wire served as the counter electrode and reference electrode. It was prepared by submerging the silver in bleach for five minutes to coat the silver with a thin layer of silver chloride (AgCl). The exact surface area is not critical for this electrode, but the surface area should be sufficiently large such that it does not interfere with reactions occurring at the gold electrode. The purpose of the counter electrode is to provide a path for the electrons to flow and serve as a reference for the voltage applied at the gold electrode [6].

The gold wire was coated in candle wax for insulation and to ensure a constant exposed gold surface area. Before the wax was applied, the gold wire was soaked in nitric acid to remove impurities that may interfere with the oxygen reaction at the surface. Once the electrode was cleaned, it was coated in candle wax. A plain beeswax tealight was melted, and one end of the gold electrode was submerged in the wax. To avoid the electrode separating from the wax when it cooled, the electrode was submerged long enough to reach the same temperature as the melted wax before being taken out. To expose the wax-coated end of the electrode, the tip could be cut with a sharp blade because gold is a relatively soft metal. The resulting surface of the gold electrode had a diameter of approximately 0.5 mm. In order to minimize the wax that may have coated the exposed tip in the cutting process, the blade first cut all the way around the wax layer before being cleaned and used to carefully cut through the gold (in the same path that was left after cutting through the wax). Figure 2.1 shows the gold electrode after it has been coated in wax.

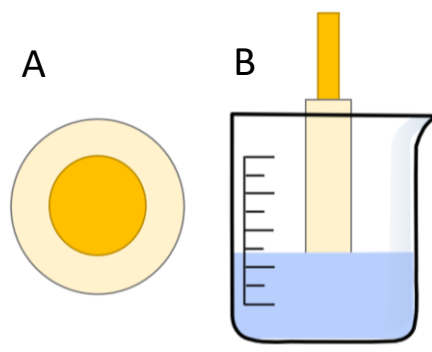


Figure 2.1 A) Bottom view of the wax-coated electrode. The wax will ensure that the surface area of exposed gold remains constant for each experiment. The wire diameter is approximately 0.5 mm. B) Depiction of how the electrode will be placed in the analyte solution.

The purpose of the wax is to leave a constant area of gold exposed; therefore, having a clean surface will make it easier to estimate the surface area at which the oxygen reduction reaction occurs, which is important for estimating the expected current magnitudes and resistances. After coating the electrode in wax and carefully cutting off the tip of the coated electrode, it was polished by rubbing the electrode on paper in a figure eight motion with the face of the exposed gold parallel to the paper [11].

2.2. Fabrication of Micro-Electrode Array

The MEA dissolved-oxygen chips were fabricated in-house by graduate students in the Minot research group using photolithography and metal deposition techniques. Figure 2.2 shows a general procedural schematic for fabricating the MEA.

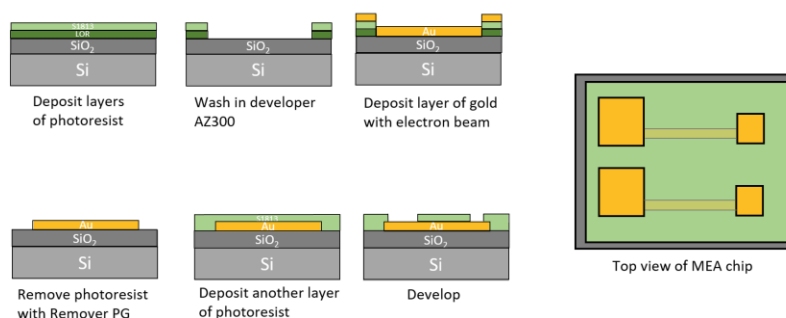


Figure 2.2 General outline of the photolithography technique used to fabricate the MEA dissolved-oxygen sensor. The aerial view schematic shows only two electrodes, while the real chip will have more.

A silicon wafer served as the base of the devices. The wafer was cleaved into chips about 2 cm x 3 cm in size. To remove residual water, the chip was placed on a hotplate at 115 °C for about 3 minutes before cooling on a cooling plate for 1 minute. A P20-primer (to promote photoresist adhesion) was dropped with a pipette onto the wafer and was left to spread across the chip for 30 seconds before being spin-coated at 4000 RPM for 45s. The resist, LOR, was then pipetted onto the center of chip and immediately spin-coated for 45 s. Following the spin-coating, the chip was placed on a hotplate at 190 C for 4 minutes for a hard bake. The purpose of the hard bake is to strengthen the resist, in this case LOR. The wafer was cooled for 1 minute after hard baking. Next, the photoresist, Shipley 1813 (positive resist), was pipetted onto center of chip and immediately spun for 30 s. Once again, the chip was hard baked on a hotplate, but this time at 115 C for 90 s before being cooled for 1 minute. A photomask with the desired pattern of chrome was placed on the wafer, with the chrome side facing the sample. The chip was exposed to UV for 3 – 4 seconds. Since the Shipley 1813 photoresist is a positive photoresist, the chemical bonds in the exposed portions will break, allowing for removal with AZ300 developer. The chip was agitated in the developer for 90 seconds to remove the exposed photoresist and underlying LOR, then dried with nitrogen gas (N₂). A schematic drawing of the photolithography process is provided in Figure 2.2.

Using an electron-beam, a chrome layer of thickness 2 nm followed by a gold layer of thickness 60 nm was deposited onto the chip with the photoresist. The chip with the layer of gold is then soaked in Remover PG to remove the remaining photoresist and LOR coated in gold. The remaining product is a chip with patches of gold, which are the working electrodes for this experiment.

2.3. Electrochemical Analysis

Cyclic voltammograms were obtained and analyzed for the wire electrode and for the MEA chip sensor. Potential sweep cycles were applied to the working electrode in the analyte solution, and the current was measured as a function of the potential against the Ag/AgCl counter electrode. To minimize noise, the experimental setup was kept in a Faraday cage.

The first experiment was done in a solution of 0.5 M potassium chloride (KCL) with a gold wire electrode. This electrode was bare gold because it was done before deciding to coat it in wax.

KCl functions as the electrolyte in the solution, which allows for current flow and limits the buildup of charge near the electrodes. The solution was at room temperature with atmospherically saturated DO concentrations. This experiment served mainly as a preliminary test to get familiar with equipment. Due to the sensitivity of dissolved oxygen measurements, it was decided that following experiments would measure potassium ferricyanide concentrations instead.

Potassium ferricyanide has a well-known electrochemical behavior, making it easier to conduct experiments with and troubleshoot the electrode design. Two experiments were done in potassium ferricyanide: one with the wax-coated gold electrode wire, and one with the MEA. For the wax wire sensor, the gold electrode and silver electrode were submerged in a beaker containing potassium ferricyanide and 0.1 M phosphate buffer to keep the pH at approximately 7. Three concentrations of potassium ferricyanide were tested: 1 mM, 5mM, and 10mM. For the MEA chip sensor, the same experiment was conducted with a drop of potassium ferricyanide solution placed on top of the chip.

A similar experiment was going to be conducted with dissolved oxygen, since the purpose of the sensor is to measure DO concentrations. However, this experiment was not completed due to COVID-19 restrictions. The general setup for the proposed DO experiment with both the wax covered electrode and the MEA chip is described in Figure 2.3. Figure 2.3 A and B show chloride ions (green) reacting with the silver electrode to produce silver/silver chloride and electrons. The produced electrons flow through the internal circuit in the direction of the red line. These electrons exit at the gold electrode to reduce the dissolved oxygen (red O_2) to yield hydroxide ion (red and white OH^-). Notice that the direction of current flow is opposite charge flow.

Although Figure 2.3 describes the reactions that take place in a DO measurement experiment, the same concept can be applied to the potassium ferricyanide experiment. Instead of oxygen reacting at the gold electrode, the potassium ferricyanide is the species that gets reduced (causing the flow of electrons).

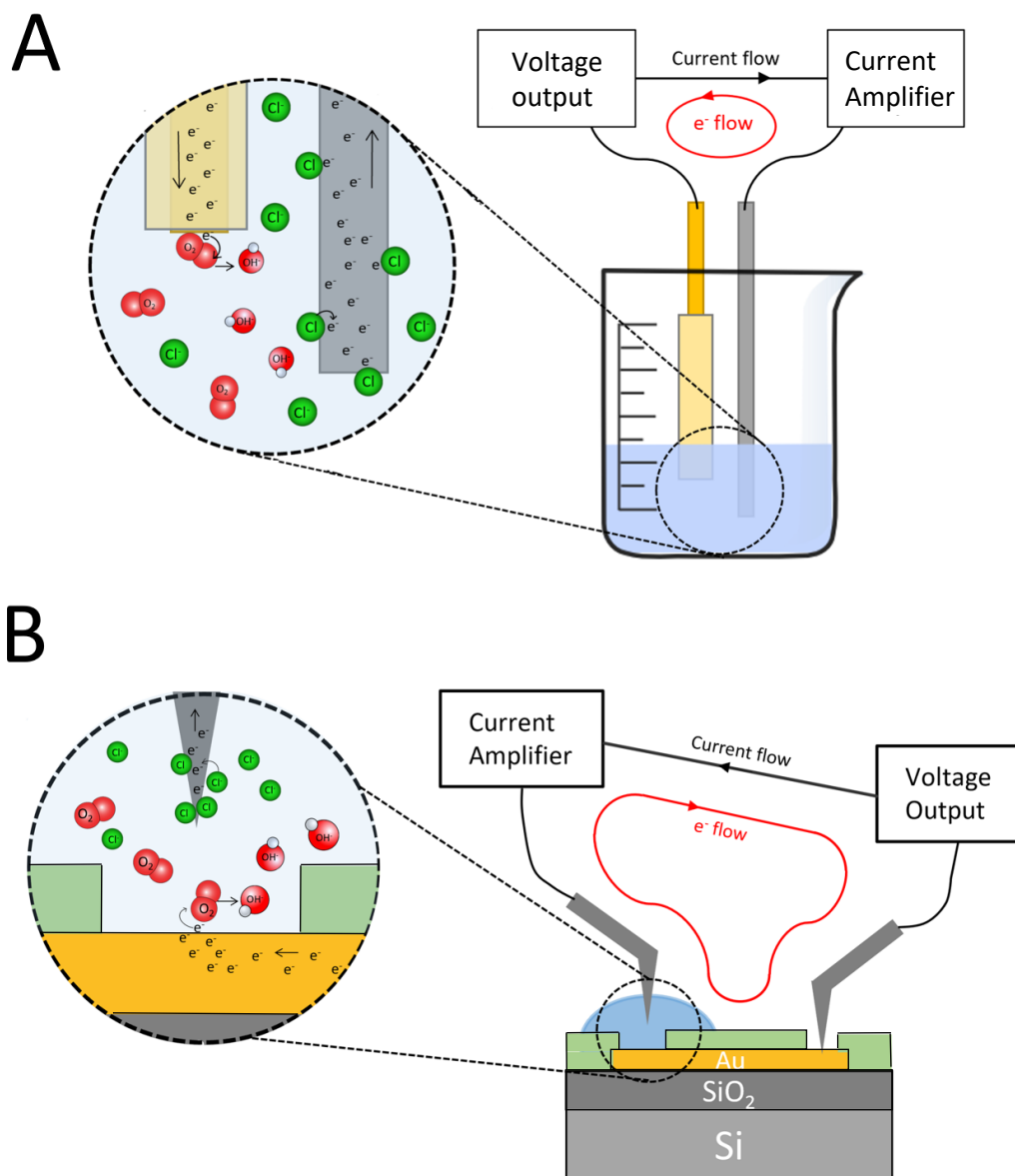


Figure 2.3 **A)** Electronic setup for the wire electrode coated in wax. A beaker is filled with the analyte solution containing KCl . The gold working electrode on the left is coated in candlewax and serves as the location for DO reduction. The electrode on the right is the silver counter electrode, where silver chloride reactions occur. **B)** Electronic setup of MEA sensor in probing station. A drop of water is placed over the gold electrode where DO gets reduced, and a silver probe tip was used as the counter electrode. The other probe tip was used to apply a potential to the gold working electrode. Both setups in **A** and **B** are inside a faraday cage to limit noise.

Chapter 3 –Results & Discussion

Experiments were run to test the reliability of the electrode setup, and to better understand how to interpret cyclic voltammograms. Initially, wax-less wire electrodes were used to gather cyclic voltammograms for DO. However, it proved difficult to control for DO concentration and to control for interference from other electrochemically active species. This led to the decision to run experiments with the well-known ferri/ferrocyanide redox couple. Because this redox couple has a known electrochemical behavior, it has become a standard for testing electrochemical equipment. The ferri/ferrocyanide redox couple is more predictable than DO, making it easier for preliminary tests of the sensors.

Before collecting the cyclic voltammograms, noise levels were recorded inside and outside of a Faraday cage to know the expected noise levels for the system, as shown in Figure 3.1.

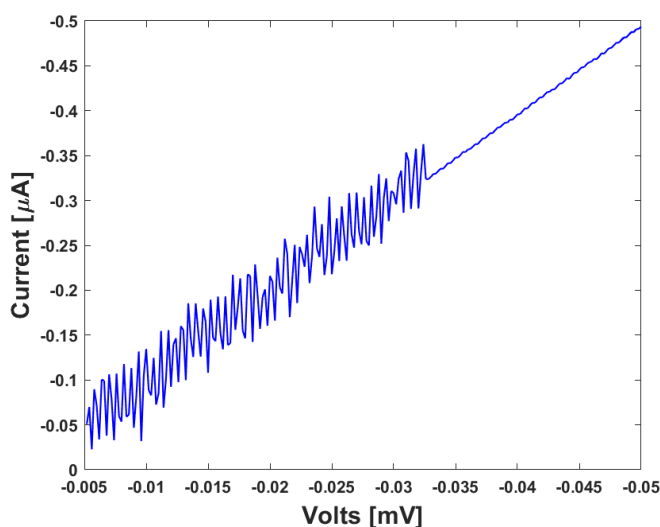


Figure 3.1 A comparison of the current noise outside and inside a Faraday cage. The noise level is significantly decreased at 0.033 V, which is when the experimental setup was placed inside the Faraday cage.

The voltage output and current amplifier were hooked up to a resistor, and the noise data was collected during one potential sweep. The graph in Figure 3.1 is linear and represents a simple graph of Ohm's law. The experimental setup was placed in a Faraday cage once the potential reached 0.033 V, which is visualized by the significant noise reduction. To keep a minimal background noise, all cyclic voltammograms for DO measurements were taken inside the Faraday cage.

3.1- Dissolved Oxygen Cyclic Voltammograms

Cyclic voltammograms were obtained from the preliminary setup at atmospherically saturated oxygen levels in a KCl solution. All measurements were done at room temperature, and the solutions remained unstirred.

Cyclic voltammograms for the initial DO experiment were collected with various sweep windows, starting with small sweep windows that increased until the oxygen reduction currents were observed. The following cyclic voltammograms were taken with a working electrode that was not covered in wax. The plots in Figure 3.2 show various graphical features that occurred during the DO experiments.

An interesting feature of Figure 3.2 A is the one cycle that shows a higher current than the rest of the cycles, which also happens to be the first cycle of that experimental trial. Normally one would see such a difference in current from varying the DO concentration. Similar results have been previously recorded in experiments where DO concentration was varied [12]. A possible explanation for the peak is that during the first cycle there was a buildup of DO around the electrode surface (because no DO had been consumed at that point). The subsequent cycles may show a lower current because the DO did not have time to replenish since the solution was unstirred. Another interesting feature is the crossover of the forward and reverse scans (except the first scan), which means that the current from the return scan is higher than that of the forward scan.

Figure 3.2 B has a similar shape to 3.2 A, but the sweep window was larger and the graph therefore shows data beyond -0.5 V. Figure 3.2 B also shows slightly higher currents than Figure 3.2 A in the comparable region of 0 to -0.5 V, which is likely be due to the inability to control for electrode surface area without the wax coating.

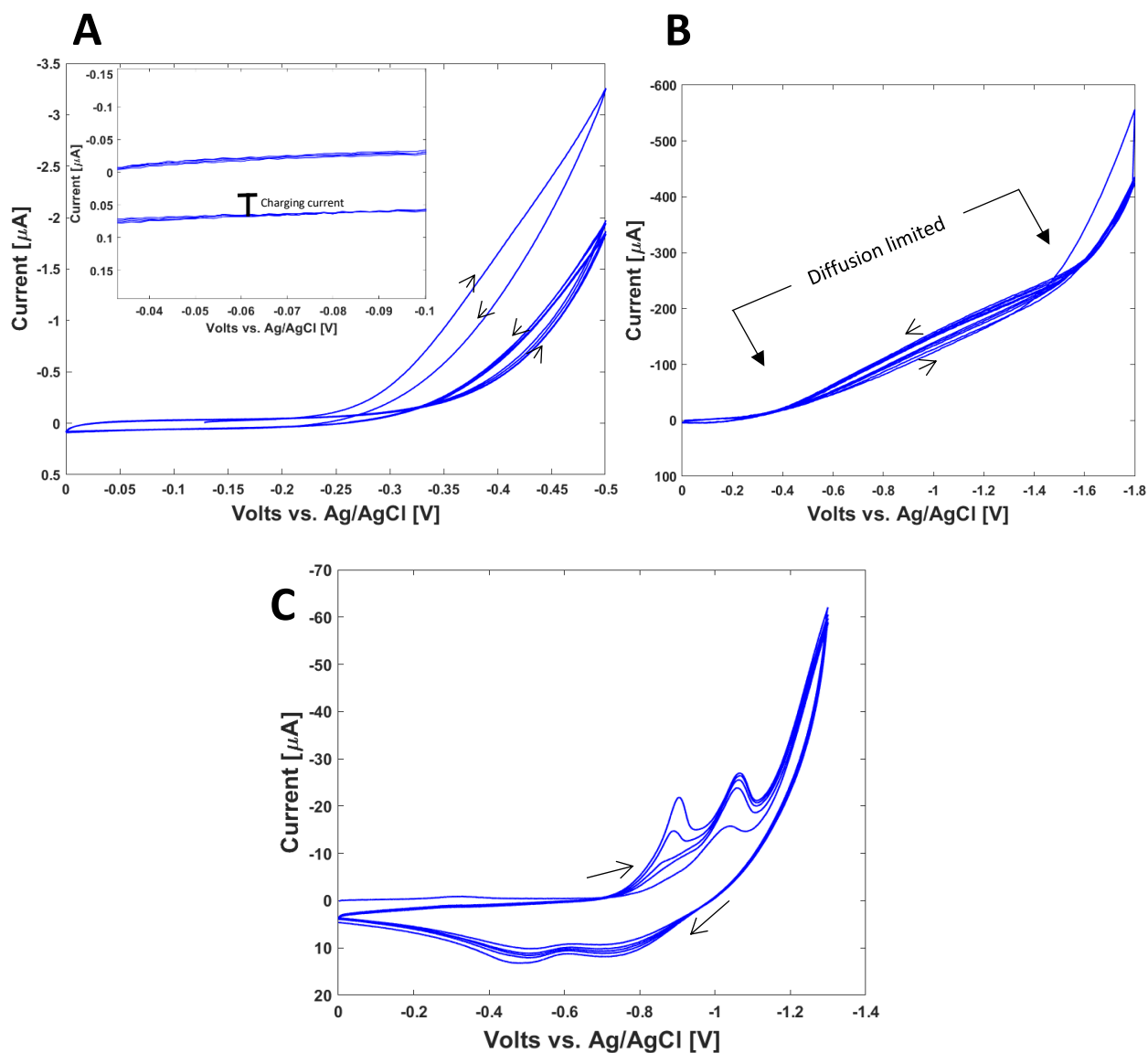


Figure 3.2 Cyclic voltammograms in unbuffered 0.5 M KCl solutions at room temperature and atmospheric conditions. Arrows indicate direction of scans. **A)** The current observed when a voltage is cycled from 0 V to -0.5 V at 50 mV/s. *Inset:* Zoom on the graph for -0.03 V to -0.1 V, where the charging current is half of the distance between the cathodic and anodic sweep. **B)** The current observed when a voltage is cycled from 0 V to -1.8 V at 200 mV/s. The diffusion limited (polarized) region is labeled. **C)** The current observed when a voltage is cycled from 0 to -1.3 V with a sweep rate of 200 mV/s. A new silver wire electrode was used. The general shape of this voltammogram is consistent with each cycle, except the peaks at about -0.85 V and -1.05 V which progressively get larger with each cycle.

Another feature in Figure 3.2 B is that since the sweep window is larger, it includes electrochemical behavior beyond the diffusion limited region. There is another sharp increase in current at about -1.6 V, which is likely due to other reactions occurring.

Both graphs in Figures 3.2 A and B appear to enter the faradaic current region at about -0.2 V, which is the region at which currents are caused by the reduction of DO. Before -0.2 V, the current is only caused by the charging current from the double layer capacitance. This region is shown up close in the inset of Figure 3.2 A. This double layer capacitance can be estimated from the equation

$$I = C \frac{dV}{dt}, \quad (5)$$

where C is the double layer capacitance, I is the charging current, and $\frac{dV}{dt}$ is the sweep rate.

From Figure 3.2 A, the charging current can be estimated to be $0.04 \mu\text{A}$ and $\frac{dV}{dt}$ was

50 mV/s . Solving for the double layer capacitance, we get

$$C = \frac{4 \times 10^{-8} \text{ A}}{0.05 \text{ V s}^{-1}} = 0.8 \mu\text{F}. \quad (6)$$

This double layer capacitance is reasonable for a gold electrode with a surface area on the order of 1 mm^2 ($80 \mu\text{F/cm}^2$). The literature values for similar capacitors are between $10 \mu\text{F/cm}^2$ to $40 \mu\text{F/cm}^2$ [13]. The small discrepancy between the calculated value and the literature values is possibly due to the rough estimate of the electrode surface area, since there was no wax coating on this electrode to control for the area.

Another cyclic voltammogram was collected on a later day with the same external conditions as the experiment used for Figure 3.2. The new data is represented in Figure 3.2 C, and this graph looks quite different from the graphs A and B, despite using the same external conditions.

The graphs in Figure 3.2 A and B are relatively smooth, which suggests that there are no contaminants present. When a reactive contaminant is present, they may cause peaks in the graphs. Figure 3.2 C shows a cyclic voltammogram with many peaks. Although the external

environment was kept the same, one difference was that a new, clean, silver wire which had not been submerged in bleach was used as the counter electrode.

A few noticeable features in Figure 3.2 C are characteristic of electrode degradation. First, the symmetric peaks that are progressively increasing at -0.85 V and -1.05 V are indicative of redox events arising from surface-adsorbed species [14], such as silver from the counter electrode depositing onto the working electrode. Another feature is the wider peak on the return scan, which could be the desorption of the adsorbed species. It is not clear why these features were observed in Figure 3.2 C, but not in A and B.

3.2- Potassium Ferricyanide Cyclic Voltammograms

Similar to the experiments in section 3.1, cyclic voltammograms were collected for measurements involving the ferri/ferrocyanide redox couple. The first experiment was done with the wax coated electrode in a solution of 5 mM potassium ferricyanide (Figure 3.3 A) and 10 mM potassium ferricyanide (Figure 3.3 B). The diffusion limited (polarized) region appears to be between approximately 0.1 V and 0.4 V. This is the region where the curve appears to be relatively flat, and most of the current change is due to non-faradaic currents.

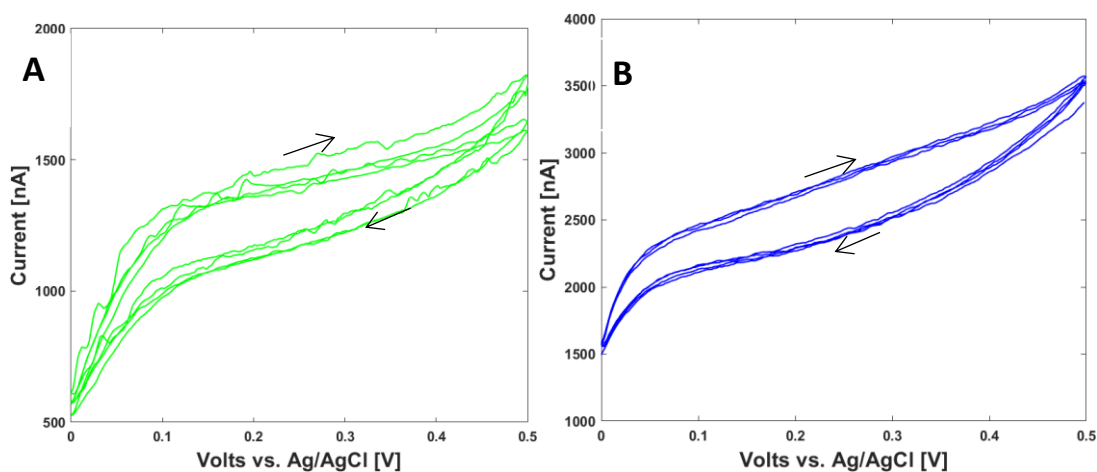


Figure 3.3 Cyclic voltammograms with the wax-coated electrode in potassium ferricyanide concentrations of **A)** 5 mM, and **B)** 10 mM. Experiments were conducted in a Faraday cage at room temperature with a sweep rate of 150 mV/s. The pH was kept near 7 with a 0.1 M solution of phosphate buffer.

In Figure 3.3, there is a clear increase in currents with a higher concentration of potassium ferricyanide. For example, when the current is 0.2 V, the bottom curve (cathodic trace) is about

1 μA with 5 mM of potassium ferricyanide, and about 2 μA for 10 mM of potassium ferricyanide. The concentration and measured current appears to be directly proportional as expected; however, more data is needed to conclude this. Due to time restrictions, experiments were shifted to the MEA after seeing the expected increase in current with concentration from Figure 3.3.

The same experiment that was done with the wax-covered electrode was done with the MEA, except measurements were done in 1 mM potassium ferricyanide in addition to 5 mM and 10 mM. The sweep window was extended for this experiment to see the electrochemical behavior from a wider range of potentials. Figures 3.4 A, B, and C show the cyclic voltammograms for 1 mM, 5 mM, and 10 mM, respectively.

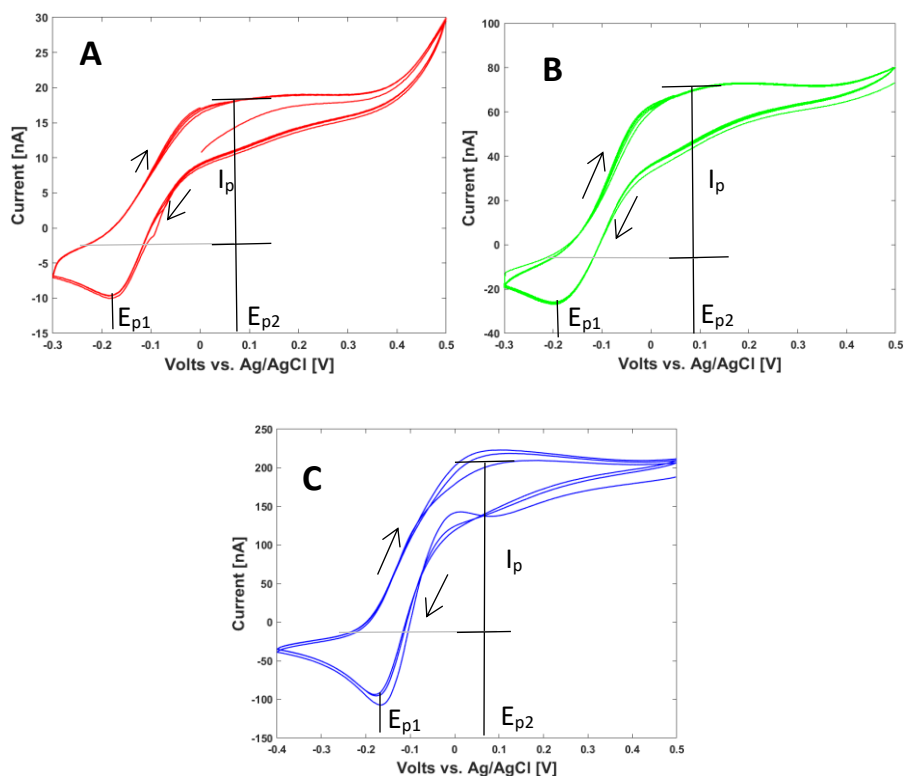


Figure 3.4 Cyclic voltammograms with the MEA sensor in potassium ferricyanide concentrations of **A)** 1 mM, **B)** 5 mM, and **C)** 10 mM. Experiments were conducted in a Faraday cage at room temperature and a sweep rate of 150 mV/s. The pH was kept near 7 with a 0.1 M solution of phosphate buffer. Peak anodic current (I_p) and the voltage at the peaks (E_{p1} and E_{p2}) are labeled. The peak currents are measured from the base current which is the flat portion of the graph marked with the grey line for the anodic trace.

Once again, the current appears to increase linearly with the concentration of potassium ferricyanide. The currents in Figure 3.4 are significantly less than the currents measured in Figure 3.3, which is expected because the MEA electrode surface area ($6400 \mu\text{m}^2$) is much smaller than the wire electrode ($\sim 1 \text{ mm}^2$).

The ferri/ferrocyanide redox couple is a well-known reversible reaction, meaning that electron transfer is rapid or unhindered [15]. From the collected data in Figure 3.4, the anodic and cathodic peak currents are about the same magnitude, which is characteristic of a reversible reaction. However, the difference in voltage between peak currents ($E_{p2}-E_{p1}$) for a reversible reaction should be 59 mV, and the difference in voltage in the experimental data is closer to 200 mV. Such a stretched cyclic voltammogram is characteristic of a *quasi-reversible* reaction, which is a reaction that is neither reversible nor irreversible. A likely cause of this increased difference in voltage is that the counter electrode also served as the reference electrode, or that there was high resistance due to inadequate electrolyte concentration in the solution. Many electrochemical measurements are done with a three-electrode system, where the reference electrode is separate from the counter electrode. Because this experiment combined the counter and reference electrodes, there is an extra voltage drop that is independent of the reactions at the electrodes. Other causes of quasi-reversible behavior for reversible reactions include impurities or adsorbed species on the electrodes because it blocks the rate of electron transfer. It is important to be aware of impurities that may form during experiments. An example is the deposition of Prussian Blue onto an electrode. A paper was published that explained a method for depositing Prussian Blue onto an electrode surface by applying a constant potential in a potassium ferricyanide solution [16]. If Prussian Blue deposits onto electrodes in the presence of an applied potential, this could hinder the electron transfer at the electrode, thereby having the appearance of a quasi-reversible reaction.

Because it is well known that the ferro/ferricyanide system is reversible, the Randles-Sevcik equation can be used to predict peak currents. A theory line from the Randles-Sevcik equation (Equation 7) is plotted in Figure 3.5 B. The Randles-Sevcik equation for reversible reactions at room temperature is

$$i_p = 2.69 \times 10^5 n^{\frac{3}{2}} A C D^{\frac{1}{2}} V^{\frac{1}{2}}, \quad (7)$$

where n is the number of electrons transferred in the redox event, A is the surface area of the electrode in cm^2 , C is the concentration in $\text{mol}\cdot\text{cm}^{-3}$, D is the diffusion coefficient of the analyte in $\text{cm}^2\cdot\text{s}^{-1}$, and V is the scan rate in $\text{V}\cdot\text{s}^{-1}$. For the ferri/ferrocyanide redox reaction n is one electron, and the diffusion coefficient for ferrocyanide, D , is $6.67 \times 10^{-6} \text{cm}^2\text{s}^{-1}$ [17]. The diffusion coefficient for ferrocyanide is used because the calibration curve in Figure 3.5 B comes from the oxidation of ferrocyanide. The surface area of the electrode was $6400 \mu\text{m}^2$ ($6.4 \times 10^{-5} \text{cm}^2$), and the sweep rate was 0.15Vs^{-1} . These values predicted peak currents that were fairly close to the experimental data as seen in Figure 3.5.

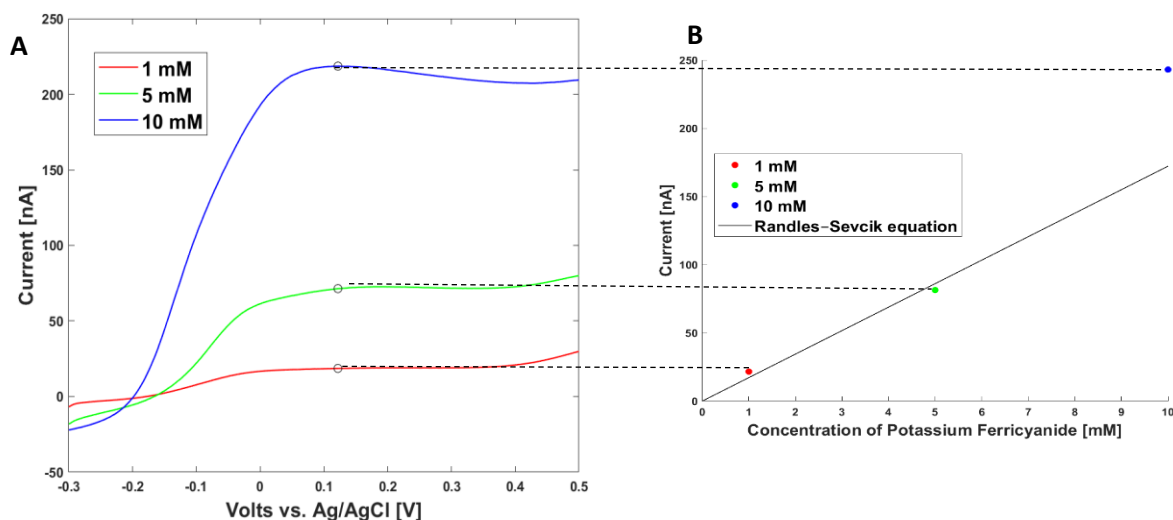


Figure 3.5 A) The anodic sweep from the data in Figure 3.5 is plotted, which represents the current from the oxidation of ferrocyanide. B) Peak current from each curve in A against its respective concentration of potassium ferricyanide. The peak current is defined as the difference between the peak and the base current, which is the flat portion at about -0.25 V. The Randles-Sevcik equation was plotted with the experimental data.

The peak currents were recorded from the anodic sweep. The currents were then plotted against their respective concentrations. The third point in the graph (10 mM) is a bit higher than expected from the Randles-Sevcik equation, which may be due to the concentration of ferricyanide or the surface area of the electrode being higher than initially thought. Due to the development of scratches or low conductivity in the electrodes, a new electrode was used for each experiment. Although every electrode was supposed to be $6400 \mu\text{m}^2$, there may have been slight variations between the electrodes.

Further evidence that supports the experimental data and the Randles-Sevcik equation is shown by predictions from mass-transfer equations. Equation 8 is the general flux equation for one-dimensional mass transfer in cartesian coordinates:

$$N_A = -D_{AB} \frac{dC_A}{dz} + \frac{C_A}{C} (N_A + N_B), \quad (8)$$

where D_{AB} is the diffusion coefficient of ferrocyanide in water, C_A is the concentration of ferrocyanide, C is the total concentration, N_A is the flux of ferrocyanide, and N_B is the flux of water (which is zero in this case). The second term can be assumed to be zero because $C_A \ll C$ for the case of 1 mM potassium ferricyanide.

Equation 8 can be reduced to

$$N_A = -D_{AB} \frac{dC_A}{dz}, \quad (9)$$

which can be integrated to get

$$N_A = \frac{D_{AB} C_A}{\delta}, \quad (10)$$

where δ is the depletion layer. Because this is a reversible reaction and electron transfer happens quickly, it is assumed that the concentration at the electrode surface is zero. The equation for the thickness of the depletion layer is

$$\delta = 2\sqrt{D_{AB}t}, \quad (11)$$

where t is the time it takes to reach 0.1 V (which is where the diffusion limited transfer occurs). This was calculated to be 0.66 s from the scan rate of 0.15 Vs⁻¹. We can solve for N_A by plugging (11) into (10) and plugging in numbers:

$$\begin{aligned} N_A &= \frac{D_{AB} C_A}{2\sqrt{D_{AB}t}} = \frac{(6.67 \times 10^{-6} \text{ cm}^2 \text{ s}^{-1})(1 \times 10^{-6} \text{ mol} \cdot \text{cm}^{-3})}{2\sqrt{(6.67 \times 10^{-6} \text{ cm}^2 \text{ s}^{-1})(0.66 \text{ s})}} \\ &= 1.6 \times 10^{-9} \text{ mol} \cdot \text{s}^{-1} \text{ cm}^{-2}. \end{aligned} \quad (12)$$

Because one electron is transferred for every ferrocyanide that gets oxidized, there is a 1:1 molar ratio. We can therefore solve for the moles of electrons per second (\dot{n}) as follows:

$$\begin{aligned}\dot{n} &= N_A A = (1.6 \times 10^{-9} \text{ mol} \cdot \text{s}^{-1} \text{ cm}^{-2}) (6.4 \times 10^{-5} \text{ cm}^2) \\ &= 1.02 \times 10^{-13} \text{ mol } e^{-} \cdot \text{s}^{-1}.\end{aligned}\tag{13}$$

We can get the current from the flow of electrons by multiplying by Avogadro's number and converting to Coulombs. This gives a current of

$$i = 9.8 \times 10^{-9} \text{ A} = \mathbf{9.8 \text{ nA}}.$$

This is on the same order of magnitude as what is predicted by the Randles-Sevcik equation, which is solved by plugging the known values into Equation 7:

$$\begin{aligned}i_p &= 2.69 \times 10^5 (6.4 \times 10^{-5} \text{ cm}^2) (1 \times 10^{-6} \text{ mol} \cdot \text{cm}^{-3}) (6.67 \times 10^{-6} \text{ cm}^2 \text{ s}^{-1})^{\frac{1}{2}} (0.15 \text{ V s}^{-1})^{\frac{1}{2}} \\ &= 17 \times 10^{-9} \text{ A} = \mathbf{17 \text{ nA}}.\end{aligned}$$

The calculated values do not perfectly match because there were several simplifying assumptions made for the mass transfer method, such as one-dimensional transfer over the flat electrode, steady state, and dilute potassium ferrocyanide. However, both calculations support that my collected data was in the correct range of currents.

The results are further supported by an experiment from a paper that collected measurements with a bare 0.7 mm diameter gold electrode in a 5 mM potassium ferricyanide solution [18]. The peak current from their cyclic voltammogram was about 4.5 μA . Because the peak current is linearly related to the electrode surface area, a quick calculation predicted that the experimental data for a 6400 μm^2 MEA electrode in 5 mM of potassium ferricyanide (not 1 mM like in the above calculations) should have been about 75 nA, which is close to the collected experimental data of 81 nA.

Chapter 4 –Conclusion

The photolithography-fabricated micro-electrode array showed a positive linear relationship between the concentration of potassium ferricyanide and the measured current, and the data agreed with theoretical predictions. The cathodic and anodic peak currents were approximately equal, which is expected from a reversible reaction. However, the voltage difference between the location of the two peak currents was greater than what is expected from a reversible reaction. This was likely due to using a combined counter and reference electrode that added an extra voltage drop independent of the reactions at the electrodes, or that there was a higher resistance in the solution due to inadequate electrolyte concentrations. The measured peak currents for three different concentrations of potassium ferricyanide agreed fairly well with the Randles-Sevcik equation. A second method was used for predicting the peak currents based on a first principles mass transfer approach. This prediction agreed with both the experimental data and the Randles-Sevcik equation. These predictions were further supported by literature [18].

The experiment involving wire electrodes and dissolved oxygen did not result in a calibration curve because of difficulties with controlling the concentration. However, the atmospherically saturated solutions gave insight into expected cyclic voltammogram shapes, and factors that may interfere with the measurements. Reasonable double-layer capacitance was calculated for the wire electrode, and differences in the slopes with respect to applied voltage was observed. A graph with many peaks in the current was also collected, which helped identify possible interfering factors.

In future work, it would be beneficial to continue testing the micro-electrode array in ferricyanide solution to get consistent and reproducible data that strongly agrees with the Randles-Sevcik equation. A consistent correlation between concentration and current is essential for being able to predict concentrations in solution. Once this is obtained with the ferri/ferrocyanide experiments, the focus can be shifted toward applying our knowledge to dissolved oxygen experiments. Further research is also needed to understand and control for the factors that interfere with the measurements. Understanding how dissolved oxygen interacts with the micro-electrode array sensor will allow for future applications in monitoring living systems such as biofilms.

Acknowledgements

I would like to thank my thesis advisor, Dr. Ethan Minot, because this project could not have been completed without his extensive guidance, direction, and support. I would also like to thank Dr. Janet Tate for providing valuable feedback during the writing process. I would like to thank graduate students Mitch Senger, Carly Fengel, and Dublin Nichols for valuable discussion, fabrication of the MEA, and laboratory guidance. Lastly, I would like to thank Dr. Zhenxing Feng for supplying potassium ferricyanide, and Dr. Clare Reimers for advice and valuable discussion.

References

- [1] J.-H. Lee, Y. Seo, T.-S. Lim, P. L. Bishop, & I. Papautsky, “MEMS Needle-type Sensor Array for in Situ Measurements of Dissolved Oxygen and Redox Potential”, *Environmental Science & Technology*, 41(22), 7857–7863. (2007)
- [2] R. Wang, H. Yu, Z. Li , “Microelectrode Array”, *Micro Electro Mechanical Systems. Micro/Nano Technologies*, vol 2. Springer, Singapore. 1-33. (2018)
- [3] R. C. Kelly, M. A. Smith, J. M. Samonds, A. Kohn, A. B. Bonds, J. A. Movshon, & T.S. Lee, “Comparison of Recordings from Microelectrode Arrays and Single Electrodes in the Visual Cortex”, *Journal of Neuroscience*, 27(2), 261–264. (2007)
- [4] K. Sauer, A. H. Rickard, & D. G. Davies, “Biofilms and Biocomplexity”, *Microbe Magazine*, 2(7), 347–353. (2007)
- [5] Fondriest Environmental, Inc. “Measuring Dissolved Oxygen”, Fundamentals of Environmental Measurements. (2014). Web. <https://www.fondriest.com/environmental-measurements/measurements/measuring-water-quality/dissolved-oxygen-sensors-and-methods>.
- [6] N. Elgrishi, K. J. Rountree, B. D. Mccarthy, E. S. Rountree, T. T. Eisenhart, & J. L. Dempsey, “A Practical Beginner’s Guide to Cyclic Voltammetry”, *Journal of Chemical Education*, 95(2), 197–206. (2017)
- [7] “Cyclic Voltammetric Study of ferrocyanide/ferricyanide Redox Couple” [DOCX]. Moorhead: Minnesota State University.
- [8] I. Fatt, “Polarographic Oxygen Sensor: Its Theory of Operation and Its Application in Biology, Medicine, and Technology”, Ohio: CRC Press. (1976)
- [9] G. W. Luther, B. T. Glazer, S. Ma, R. E. Trouwborst, T. S. Moore, E. Metzger, ... P.J. Brendel, “Use of voltammetric solid-state (micro) electrodes for studying biogeochemical processes: Laboratory measurements to real time measurements with an in situ electrochemical analyzer (ISEA)”, *Marine Chemistry*, 108(3-4), 221–235. (2008)

- [10] S.-Y. Liu, Y.-P. Chen, F. Fang, J. Xu, G.-P. Sheng, H.-Q. Yu, ... Y.-C. Tian, “Measurement of Dissolved Oxygen and Its Diffusivity in Aerobic Granules Using a Lithographically-Fabricated Microelectrode Array”, *Environmental Science & Technology*, 43(4), 1160–1165. (2009)
- [11] J. Summers, “Potentiostat Notes 5: How to make low cost electrodes”, Public Lab. (2014). Retrieved from <https://publiclab.org/notes/JSummers/01-09-2014/potentiostat-notes-5-how-to-make-low-cost-electrodes>
- [12] J. Wang, C. Bian, J. Tong, J. Sun, Y. Li, W. Hong, & S. Xia. “Modification of Graphene on Ultramicroelectrode Array and Its Application in Detection of Dissolved Oxygen”, *Sensors*, 15(1), 382–393. (2014)
- [13] M. S. Halper, J. C. Ellenbogen, “Supercapacitors: A Brief Overview” (PDF)(Technical report). MITRE Nanosystems Group. (2006).
- [14] K. J. Lee, B. D. McCarthy, & J. L. Dempsey. “On decomposition, degradation, and voltammetric deviation: the electrochemists field guide to identifying precatalyst transformation”. *Chemical Society Reviews*, 48(11), 2927–2945. (2019)
- [15] “Inorganic Material and Metal Casse”. *Enological Chemistry*, 355-373. (2012)
- [16] A. A. Karyakin, E. E. Karyakina, & L. Gorton, “On the mechanism of H₂O₂ reduction at Prussian Blue modified electrodes”. *Electrochemistry Communications*, 1(2), 78-82. (1999)
- [17] S. J. Konopka, & B. McDuffie, “Diffusion coefficients of ferri- and ferrocyanide ions in aqueous media, using twin-electrode thin-layer electrochemistry”. *Analytical Chemistry*, 42(14), 1741-1746. (1970)
- [18] Y.-S. Choi, K.-S. Lee, & D.-H. Park, “Hybridization by an Electrical Force and Electrochemical Genome Detection Using an Indicator-free DNA on a Microelectrode-array DNA Chip”. *Bulletin of the Korean Chemical Society*, 26(3), 379–383. (2005)